TrueForce: A Compliant Method for Perceptually Aligned Interaction with ETHD-Simulated Virtual Objects

YUQI ZHOU, Purdue University, USA
VOICU POPESCU, Purdue University, USA

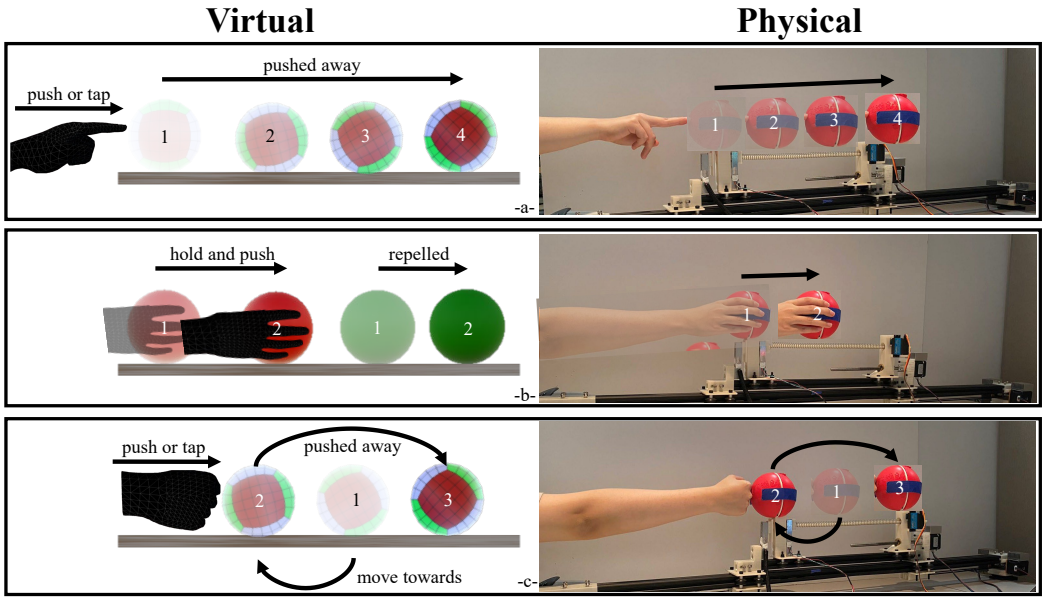

Fig. 1. An overview of our ETHD prototype implementing the TrueForce method (right) and three representative physical interaction tasks (left). Sequential frames are shown for each task. (a) The user interacts with a stationary virtual ball by tapping, poking, or pushing it; the virtual ball responds in real time based on the user's input, with the ETHD-held ball serving as the physical proxy. (b) The user holds and pushes one charged virtual ball while experiencing simulated electromagnetic forces, causing the second ball to be repelled. (c) The user intercepts and bounces back a moving virtual ball upon contact, demonstrating TrueForce's ability to safely handle dynamic object interactions

To enhance learning and training, VR haptic devices must provide safe and physically accurate feedback that helps users build intuitions about force and motion. We present TrueForce, a method for rendering force feedback by capturing user input and reconfiguring a compliant mechanism in real time to align perceived with expected forces. We implemented TrueForce in a grounded Encountered-Type Haptic Display (ETHD) and demonstrated its versatility through three representative physics scenarios: pushing a stationary object, experiencing electrostatic repulsion, and bouncing a moving object. A user study with 29 participants showed

Authors' Contact Information: Yuqi Zhou, Purdue University, West Lafayette, USA, zhou1168@purdue.edu; Voicu Popescu, Purdue University, West Lafayette, USA, popescu@purdue.edu.

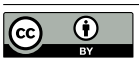

ACM 2577-6193/2026/5-ART1
https://doi.org/10.1145/3804491

that users adapted to new interaction profiles within 2–3 trials, and that rendered forces remained within perceptual thresholds except in the heaviest and most dynamic conditions. These results suggest that users can rapidly adapt to the system's force-motion mappings, providing the consistent sensorimotor feedback necessary for building physical intuitions when interacting with moving virtual objects.

CCS Concepts: • **Human-centered computing** → **Virtual reality**; **Haptic devices**.

ACM Reference Format:
Yuqi Zhou and Voicu Popescu. 2026. TrueForce: A Compliant Method for Perceptually Aligned Interaction with ETHD-Simulated Virtual Objects. *Proc. ACM Comput. Graph. Interact. Tech.* 9, 1, Article 1 (May 2026), 18 pages. https://doi.org/10.1145/3804491

1 Introduction

Virtual reality (VR) immerses users into synthetic 3D environments, replacing their real-world surroundings with computer-generated objects and scenes [1]. While VR is widely used in entertainment to create captivating experiences, it also holds significant potential in education by providing immersive learning environments [Popescu et al. 2023]. In physics education, for example, traditional methods, such as memorizing formulas, viewing static images, or watching videos, often lack the realism needed for students to make meaningful connections to real world phenomena [Popescu et al. 2023]. Unlike these traditional teaching methods, VR headsets can provide students with realistic 3D simulations of physics phenomena at low cost, safely, and anywhere [Freina and Ott 2015].

The rendering of physical processes on consumer-level VR headsets is relatively straightforward. However, using visualization alone, students and trainees often struggle to connect virtual experiences with real-world phenomena [Rutten et al. 2012]. For instance, when a 3D environment displays a 0.5 kg ball and a 5 kg ball moving with the same speed, learners may not grasp the magnitude of the momentum difference between the two balls. What is needed is the incorporation of tangible physical responses, similar to those experienced in a physics lab, allowing students to directly perceive physical properties such as mass, texture, and shape.

Wearable devices, such as gloves [2], can simulate surface properties but cannot provide the strong resistance required for object collisions. A different solution, which this paper focuses on, involves grounded Encountered-Type Haptic Displays (ETHDs). These devices use mechanical actuators to align physical objects with their virtual counterparts, enabling the provision of strong resistance forces [Mercado et al. 2021].

Grounded Encountered-Type Haptic Displays (ETHDs) have been extensively studied for simulating stationary objects [Mortezapoor et al. 2023; Suzuki et al. 2020], but their application to moving virtual objects presents significant safety and interaction challenges. To simulate moving objects, the ETHD must continuously reposition itself to maintain alignment with the virtual object, increasing the risk of unintended collisions with the user's hand [Mercado et al. 2022]. Although various strategies have been proposed to mitigate such risks, such as warning the user [Mercado et al. 2022], a more desirable solution is one that allows users to safely and directly interact with moving virtual and physical objects.

Existing grounded ETHDs, such as robotic arms with integrated force/torque sensing (e.g., Universal Robots UR20 [3]), can deliver strong and precise forces. However, most existing ETHDs focus on rigid contact rendering and proxy alignment, and typically do not dynamically adjust compliance or force profiles during user interaction. This rigidity makes them effective for static or

[1] https://www.oculus.com/
[2] https://haptx.com/
[3] https://www.universal-robots.com/products/ur20/

predefined contacts, but less suitable for safe, compliant engagement with moving virtual objects or virtual objects like balls, levers, or soft surfaces within VR simulations intended for education. Additionally, the mechanical inertia and scale of industrial robots introduce safety concerns for direct hand-interaction, limiting their suitability for broad deployment in classroom learning environments [Slater 2009].

To address these challenges, we present **TrueForce**, a method designed to extend existing grounded haptic devices, such as robotic arms, to better support soft, dynamic physical replicas of moving virtual objects. TrueForce integrates a compliant spring-based mechanism with real-time force adjustment, enabling the physical rendering of soft-contact interactions that adaptively match virtual object properties. Our current implementation focuses on 1D motion and single-axis force rendering. This design choice isolates key physical variables for the learner but introduces a hardware-imposed constraint on the 3D expressive potential of VR. While the method is conceptually extensible to 3D, this prototype serves as a foundational study in how a compliant mechanism can align perceived and expected forces within a constrained interaction space. By incorporating TrueForce, traditional grounded ETHDs, such as robot arms [4], can be transformed to deliver more natural, safe, and effective interactions, making them suitable not only for static object simulation but also for dynamic, force-based VR experiences.

To demonstrate its versatility and effectiveness, we conducted a within-subject user study (N = 29) comprising three experiments. The first experiment validated the physical interaction behavior when pushing away a stationary virtual ball (Fig. 1*a*). The second experiment examined the simulation of electromagnetic forces between two charged virtual balls (Fig. 1*b*). The third experiment evaluated the interaction dynamics when bouncing back a moving virtual ball (Fig. 1*c*).

The key contributions of this work are:

- **TrueForce**, a compliant method for aligning expected and perceived forces during direct hand interaction with virtual objects.
- **Design and Assembly** of a grounded ETHD prototype that implements the **TrueForce** method to support soft, dynamic interactions in VR.
- A three-experiment user study (N = 29) demonstrating the system's ability to safely render diverse force profiles, with participants successfully adapting to the novel compliant hardware.

2 Related Work

Delivering realistic physical sensations in VR has long been a research goal. Two major approaches have emerged: (1) wearable and handheld haptic devices that provide on-body feedback (Sec. 2.1), and (2) Encountered-Type Haptic Displays (ETHDs) that present external physical proxies aligned with virtual content (Sec. 2.2). Our work builds upon these strategies but specifically addresses the challenge of enabling **safe, compliant, real-time interaction with moving virtual objects**, which prior ETHDs and grounded robots do not fully solve.

2.1 Wearable and Handheld Haptic Devices

Wearable devices enable users to experience various tactile properties directly on their bodies. Techniques include simulating temperature [Mazursky et al. 2024], texture [Shen et al. 2023], and shape through muscle stimulation [Lopes et al. 2015]. Devices like Springlets [Hamdan et al. 2019] and ArmDeformation [Lin et al. 2024] apply skin-stretch to enhance realism, while electrotactile gloves [Tanaka et al. 2023] provide additional tactile cues.

Handheld props further improve immersion by dynamically simulating object properties [Zhou and Popescu 2023]. Shifty [Zenner and Krüger 2017] shifts internal weight distribution to simulate

[4]https://www.universal-robots.com/products/ur20/

changing mass centers, and MobileGravity [Kalus et al. 2024] adjusts object weight dynamically in mobile VR settings.

While these devices excel at representing textures, local deformations, and lightweight object cues, they cannot reproduce external blocking or sustained resistance against the environment, such as stopping a rolling ball.

2.2 Encountered-Type Haptic Displays (ETHDs)

ETHDs physically align external proxies with virtual content, enabling users to touch virtual objects without continuously wearing or holding devices [Mercado et al. 2021]. Ungrounded ETHDs, such as drone-based systems [Chen et al. 2024; Herdel et al. 2022; Huppert et al. 2021], provide unmatched spatial flexibility but are constrained by payload capacity, stability, and battery life, which limits their ability to deliver strong or sustained forces.

Grounded ETHDs, including robotic arms and mobile robot platforms, can provide large, stable resistive forces with high positional accuracy [Zhou and Popescu 2025]. Robotic arms offer six degrees of freedom and can simulate a variety of tactile experiences by swapping end-effectors [Kim et al. 2020; Mercado et al. 2019; Posselt et al. 2017]. Mobile platforms extend the reach of grounded robots either through tracks [Dai et al. 2022] or mobile bases [Mortezapoor et al. 2023].

However, **most existing ETHDs focus on rigid contact rendering** and proxy alignment. They typically do not dynamically adjust compliance or force profiles during user interaction. This rigidity makes them effective for static or predefined contacts, but less suitable for safe, compliant engagement with moving virtual objects.

2.3 Grounded Haptic Interfaces with Force Feedback

Through stylus-held interactions, grounded haptic interfaces such as the PHANToM [Massie et al. 1994; Silva et al. 2009] enable users to feel virtual textures, surfaces, and localized forces with high fidelity. However, they are not designed to act as dynamic physical proxies representing the full-body motion of virtual objects, and cannot easily support interactions with moving content across larger spatial areas.

2.4 Safe Interaction with ETHDs

Ensuring safe interaction when ETHDs move dynamically in shared spaces has been a longstanding concern. Prior strategies include distancing the device when idle [Mortezapoor et al. 2023], providing visual or auditory warnings [Mercado et al. 2020, 2022], and predicting potential collision zones to adapt robot trajectories [Bouzbib and Bailly 2022]. While effective for collision avoidance, these approaches focus on preventing contact rather than supporting direct, compliant engagement during interaction.

2.5 Summary and Positioning of Our Work

Prior grounded ETHDs and haptic interfaces have demonstrated strong resistive feedback, but mainly emphasize rigid, static interactions or handheld fine-motor control. Existing safety strategies likewise prioritize avoidance over natural contact. In contrast, **TrueForce** augments grounded devices with passive compliance and real-time force adjustment, enabling perceptually aligned, physically realistic interactions with moving virtual objects. This contribution addresses a gap in prior ETHD research by supporting dynamic tasks where users directly experience forces through compliant contact.

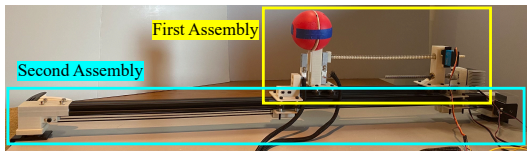

Fig. 2. Overview of the **TrueForce** system, showing the first and second assemblies.

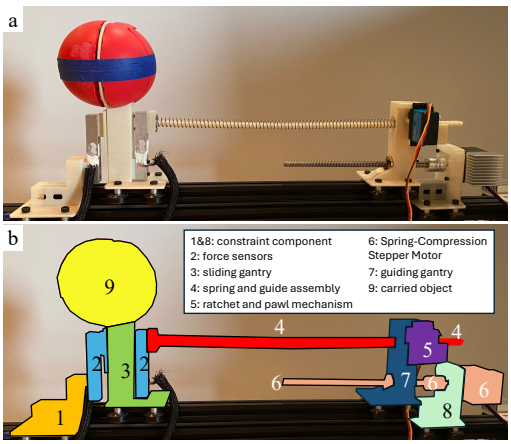

Fig. 3. First assembly detail, illustrating the compliant spring mechanism and force sensing structure.

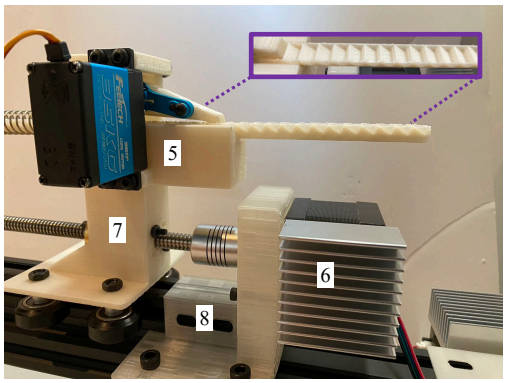

Fig. 4. Component #5 of the first assembly: The ratchet and pawl mechanism used to lock the spring assembly in place.

3 TrueForce: Method and System Design

3.1 Overview and Motivation

We designed and implemented a two-assembly haptic system based on the **TrueForce** method. The first assembly (Sec. 3.2) uses a spring-loaded mechanism to simulate mass-dependent resistance, while the second assembly (Sec. 3.3) enables positional control for aligning the device with virtual objects. The system supports both stationary and moving virtual objects. An overview of the hardware system is shown in Fig. 2.

3.2 First Assembly: Soft-Contact and Force Sensing

The first assembly of our system (Fig. 3) is responsible for enabling compliant physical interaction and measuring user-applied forces. Its main components and functions are:

- **Force Sensor Group (#2)**: A linear load cell mounted on a sliding gantry (#3) measures the user's applied force. The user pushes against a high-density foam ball (#9) attached to the gantry.
- **Spring and Guide Assembly (#4)**: A spring located between the load cell and a fixed guide (#7) allows for controlled compression during interaction. The spring smooths force transmission, mitigating sudden impacts and enabling soft-contact behavior, inspired by automotive shock-absorbing systems.
- **Spring-Compression Stepper Motor (#6)**: A Nema 17 stepper motor drives a lead screw to adjust the pre-compression of the spring independently of user input. By modifying the initial spring compression, the system can simulate varying resistance profiles depending on the mass or inertia of the virtual object.

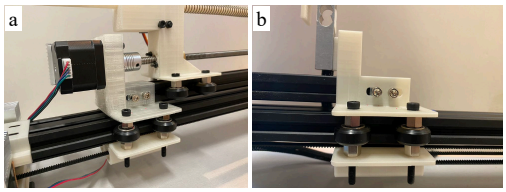

Fig. 5. Close-up of the belt-driven connection between the first and second assemblies. Two belt gantries support and move the first assembly along the rail.

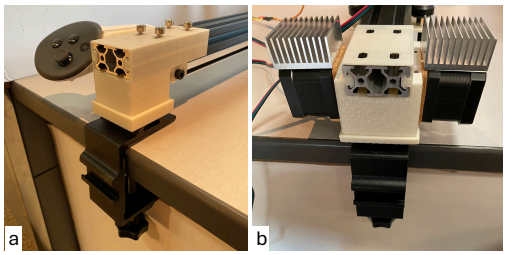

Fig. 6. Overview of the second assembly. The linear rail is rigidly secured by two desk clamps. One end holds the stepper motors driving the belt system, while the other end houses the calibration controller mount and pulleys.

- **Ratchet and Pawl Mechanism (#5 in Fig. 4)**: A servo-actuated ratchet locks the spring compression dynamically during interaction transitions. This prevents the object from rebounding after contact is released, ensuring consistency between visual and physical feedback.

3.3 Second Assembly: Repositioning Mechanism

The second assembly dynamically repositions the first assembly along a horizontal linear rail to align with moving virtual objects. Its main components and functions are:

- **Belt-Driven Gantries (Fig. 5*b*):** Two belt-connected gantries are mounted to the ends of the first assembly. These gantries ride along a rigid linear rail clamped to the work surface. Coordinated stepper motor control allows the entire first assembly (and thus the foam proxy) to translate smoothly across the plane.
- **Dual Stepper Motor Drive (Fig. 6*b*):** Two NEMA stepper motors are mounted at one end of the rail to drive the belts. The opposite end contains passive pulleys and a fixed mount for a VR controller used in calibration.
- **Real-Time Position Tracking:** The position of the foam ball proxy (#9) is computed using encoder readings and force sensor data:

$$P_{\#9} = P_{\text{initial}} + (P_{\text{first assembly, current}} - P_{\text{first assembly, initial}}) - \frac{F_{\text{load cell}}}{k}$$

  where k is the spring constant. This equation accounts for gantry displacement and spring compression, enabling accurate real-time physical-to-virtual alignment.
- **VR-Aligned Calibration (Fig. 6*a*):** A one-time calibration is performed using a VR controller mounted on the second assembly. This step maps the device's physical workspace to the virtual environment for consistent proxy alignment.
- **Force-Based Adjustment:** During interaction, the second assembly modulates the proxy's position based on force discrepancies. If the virtual target force f_t is greater than the measured force f_m, the first assembly is advanced forward to increase spring compression. If $f_m > f_t$, it retracts slightly to relieve pressure. This dynamic adjustment preserves the illusion of continuous, compliant contact with virtual objects.

The control loop minimizes the difference between measured and target force by adjusting spring compression and proxy position in real time. A 0.5 N compliance threshold is used to trigger adjustments, ensuring sensitivity without overreacting to noise [Jones 2003].

3.4 Safety Mechanisms

TrueForce integrates several passive and active safety features:

- **Compliant Spring Contact**: The primary mechanism for absorbing stiff impacts.
- **Ratchet Locking:** Locks the spring to prevent rebound and maintain physical-virtual alignment.
- **Force Monitoring and Limiting**: Caps excessive user-applied forces through real-time feedback control.

These safety mechanisms enable **TrueForce** to support direct physical interaction even during dynamic object motion, rather than relying solely on collision avoidance strategies.

3.5 System Characterization

We characterized the **TrueForce** system to evaluate its operational capabilities. These specifications were derived from our target educational scenario: simulating safe, desktop-scale hand interactions with lightweight objects (e.g., 100–600 g masses) moving at moderate indoor speeds.

- **Maximum Renderable Force:** 14 N at the contact point. This limit is sufficient to simulate the peak inertial resistance of a 600 g object accelerating rapidly from rest, or a strong electrostatic repulsion, while remaining safely within human comfort thresholds for unexpected impacts.
- **Maximum Linear Speed:** 0.25 m/s along the rail. This accommodates the deliberate, exploratory hand movements typical in educational VR tasks.
- **Force Sensing Resolution:** 0.01 N.
- **End-to-End Response Delay:** 10 ms from force sensing to actuation. This fast control loop ensures force updates occur well below human haptic perception thresholds for soft contact.
- **Effective Workspace:** 0.5 m horizontal range.
- **Backlash:** Less than 0.1 mm in the second assembly.

4 User Study

4.1 Overview and Goals

We conducted a within-subject user study to evaluate TrueForce's ability to support physically realistic and safe interactions with virtual objects. The study was approved by the Institutional Review Board of our university and involved three types of interaction tasks: (1) pushing a stationary virtual ball, (2) experiencing simulated electromagnetic repulsion between two charged balls, and (3) bouncing back a moving ball.

Our goals were to assess whether TrueForce enables users to accurately perceive different force profiles, to adapt to both static and dynamic virtual objects, and to maintain safe and comfortable interactions across a variety of physical scenarios.

4.2 Participants

Twenty-nine participants (age range 19–28 years) were recruited from the university community. All participants had normal or corrected-to-normal vision, and reported no motor impairments. Each session lasted approximately 15 minutes.

4.3 Apparatus and Setup

Participants wore a Meta Quest 3 headset for visual immersion and interacted physically with the TrueForce ETHD device, which was positioned on a desk in front of them. The VR environment displayed virtual objects aligned with the TrueForce device's physical proxy. During the experiments, participants used their dominant hand to interact directly with the physical foam ball carried by

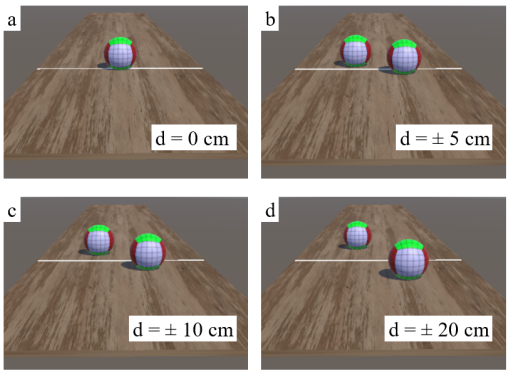

Fig. 7. Reference illustrations shown during experiments. Participants aimed to stop the ball at the white line, with example outcomes at different deviations.

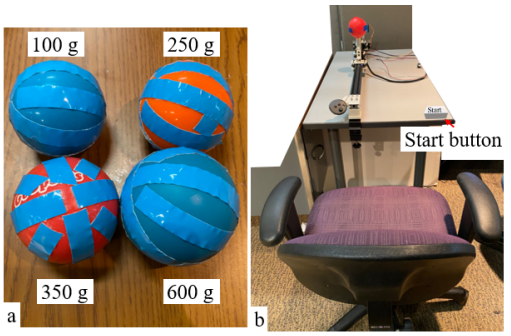

Fig. 8. (a) Real-world foam balls used in Experiment 1 perceptual comparison, taped to equalize rolling friction. (b) Full experimental setup, including the TrueForce device, chair, and participant starting position.

the device. To eliminate auditory cues from the device mechanisms, although not visible in the demonstration video, participants wore noise-canceling earbuds and listened to ambient music throughout the session.

All haptic interactions in our study were restricted to the horizontal plane to isolate inertial and repulsive forces from gravity. Because humans typically estimate an object's mass by lifting it vertically against gravity, the absence of this vertical weight as a perceptual baseline may have influenced their mass judgments. Future studies should investigate how substituting horizontal inertia for vertical weight affects mass perception in VR.

4.4 Procedure

Each participant completed three experiments in fixed order: pushing a stationary ball, repelling a charged ball, and bouncing back a moving ball. Within each experiment, participants performed a series of trials under different force or mass conditions.

At the start of each experiment, participants were given a brief training session to familiarize themselves with the task and system behavior. Trials were grouped by conditions, and conditions were presented in randomized order where applicable. Short breaks were provided between experiments to minimize fatigue.

4.5 Experiment 1: Pushing a Stationary Ball

4.5.1 Purpose and Hypothesis. This experiment evaluated TrueForce's ability to render realistic inertial feedback for static objects with varying masses. We hypothesized that participants would perceive these differences and adjust their input to stop the virtual object near a visible target. Although the virtual balls were visually identical prior to interaction, users could rely on both the haptic resistance experienced during the push and the resulting visual kinematics (e.g., how far the ball rolled) to adapt their strategy across trials.

4.5.2 Task Design and Conditions. Participants' task was to push the ball toward a white line placed at a fixed distance (50, 60, or 70 cm) along a virtual wooden surface. The goal was to stop the ball as close as possible to the line. No numerical feedback was provided; users learned through repeated interaction.

Fig. 7 shows sample outcomes at different distance errors. A perfect stop places the ball on the line (*a*), while overshooting or undershooting is visualized as deviations of ±5 cm (*b*), ±10 cm (*c*), and ±20 cm (*d*).

Three ball masses were tested: 100 g, 350 g, and 600 g. The balls were visually identical and presented in randomized blocks. Each block included 15 trials (5 per line distance), totaling 45 experimental trials. An initial training block with a 250 g ball allowed participants to explore the task.

To support training and post-condition comparisons, four physical balls were prepared with matching sizes but different masses: 100 g, 250 g, 350 g, and 600 g. The 250 g ball was used in the training block, while the other three were randomized during the experiment. All balls were equal in size (7 cm diameter), and their centers of gravity were centered. Tape was applied uniformly across all balls to normalize rolling friction. Fig. 8 shows the four balls and the experimental setup.

4.5.3 Interaction Procedure. Each trial began with the device aligning the first assembly to the virtual ball's starting location. The system unlocked the pawl, compressed the spring to simulate static friction, and tared the load cell. Participants were instructed to begin with their hand near their body and use a poke, push, or gentle tap to move the ball. Once the applied force exceeded static friction, the virtual ball detached and rolled. TrueForce dynamically adjusted its spring compression in real time to maintain appropriate resistance. The pawl re-engaged once the ball detached to prevent rebound. Fig. 9a illustrates this sequence across real-world (a, c, e, g) and virtual views (b, d, f, h).

4.5.4 Modeling and Feedback Rendering. Force feedback was computed based on real-time measurements and physical simulation. The measured force f_m was captured by the load cell, while the target force f_t was computed from estimated hand acceleration and rolling resistance:

$$f_t = ma^{\text{hand}} + \mu_r mg$$

Acceleration was estimated from position samples using a central difference method:

$$a^{\text{hand}} = \frac{\left(\frac{P_3-P_2}{t_3-t_2} - \frac{P_2-P_1}{t_2-t_1}\right)}{\frac{t_3-t_1}{2}} \tag{1}$$

To update the virtual ball's state, we derived velocity and position using:

$$v^{\text{new}} = v^{\text{prev}} + \frac{a^{\text{prev}} + a^{\text{new}}}{2}\Delta t \tag{2}$$

$$P^{\text{new}} = P^{\text{prev}} + v^{\text{prev}}\Delta t + \frac{(2a^{\text{prev}} + a^{\text{new}})\Delta t^2}{6} \tag{3}$$

4.5.5 Results and Data Analysis.

Force Feedback Fidelity. Fig. 9b compares the computed target force f_t, based on hand acceleration, with the measured force f_m from the load cells, for three ball masses. For the 100 g and 350 g balls, the measured force successfully reaches the peak of the expected curve. However, there is a noticeable initial lag (e.g., at $t = 0$ for the 350 g condition, f_t is significantly higher than f_m). This gap occurs because the motor requires a brief window (50–100 ms) to physically compress the spring from its resting state to match the sudden onset of the target force. Once this initial inertia is overcome, the system provides compliant and reactive physical resistance. However, for the 600 g condition, the system underperforms: although the simulation demands a peak target force (f_t) of 14 N, the measured force (f_m) only reaches approximately 11 N. This gap occurs because the ETHD's maximum movement speed ($0.25\ m/s$) restricts how quickly the spring can compress

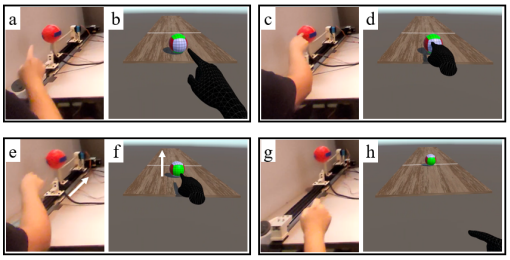

(a) Trial flow in Experiment 1: (a–b) contact; (c–d) force application; (e–f) detachment; (g–h) ball rolls to stop.

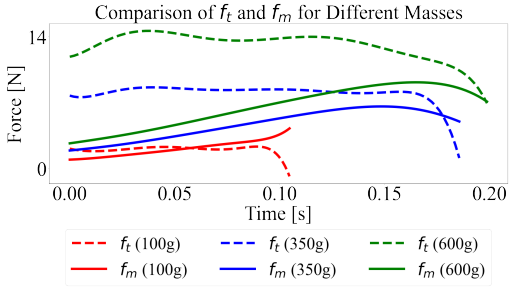

(b) Comparison of target force f_t and measured force f_m. The gap widens at higher masses due to speed constraints.

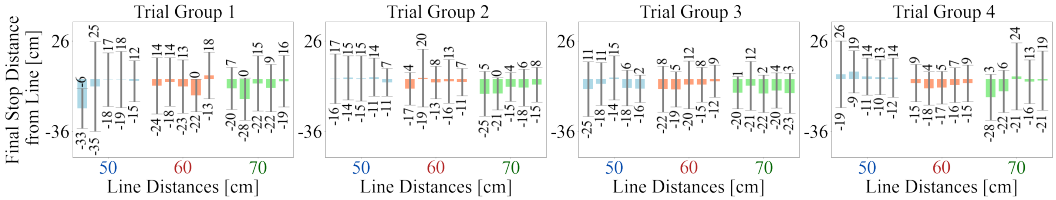

(c) Distance to target across 60 trials. Each marker represents the mean error across all 29 participants for a given line distance within that trial group, with whiskers indicating ±1 standard deviation. Trial Group 1 represents the initial 250 g training block. Error decreases as participants adapt to the haptic feedback.

Fig. 9. Experiment 1 Summary: Interacting with a stationary virtual ball. (a) illustrates the interaction sequence, while (b) and (c) present force-tracking fidelity and adaptation performance, respectively.

to match the user's rapid hand acceleration. While the hardware can statically sustain 14 N of resistance, achieving this peak dynamically within a fraction of a second exceeds the current actuator's bandwidth.

All three force profiles show a steep rise in the first 50–75 ms, corresponding to users' initial impulse to overcome static friction. In heavier conditions, sustained effort leads to a plateau, whereas lighter objects show a faster drop-off after acceleration. These patterns suggest the system can render quick onset and inertial resistance for moderate weights, but becomes less responsive under high-load conditions.

Adaptation Performance. Participants improved their performance across trials, learning to push the virtual balls closer to the target without receiving numerical error feedback. Fig. 9c shows the signed distance between the final ball position and the white line across all 60 trials, regardless of ball mass. The first 15 trials (Trial Group 1) correspond to the 250 g training block. By the third trial, most participants had reduced their error magnitude to within 20 cm of the line. This adaptation was especially prominent during the training block with the 250 g ball, where signed error significantly decreased between early and late trials ($p = 0.0075$). In contrast, no significant learning trends were observed across trials for the 100 g, 350 g, or 600 g conditions ($p > 0.05$), suggesting that TrueForce supported rapid and consistent sensorimotor calibration early in the study.

Mass Perception Accuracy. After completing the 15 interaction trials for a given mass condition, each of the 29 participants provided one overall mass estimate (yielding 29 total responses per condition). The results are shown in Tab. 1. All participants correctly identified the lightest and

heaviest balls in at least one block, indicating strong perceptual separation at extremes. However, confusion was more frequent between adjacent masses.

These results suggest that while TrueForce can support perceptual contrast between light and heavy objects, fine-grained mass discrimination remains challenging—likely due to both perceptual thresholds and physical response latency [Jones 2003].

Table 1. Mass Perception Confusion Matrix. Values represent the percentage of participants ($N = 29$) who selected each physical ball after interacting with the virtual mass condition.

	Perceived Mass (Selected Physical Ball)		
Virtual Mass	**100 g**	**350 g**	**600 g**
100 g	**93.1%**	6.9%	0.0%
350 g	20.7%	**69.0%**	10.3%
600 g	0.0%	37.9%	**62.1%**

4.6 Experiment 2: Repulsive Interaction Between Charged Balls

4.6.1 Purpose and Hypothesis. This experiment evaluated TrueForce's ability to simulate distance-dependent forces modeled after electrostatic repulsion. We hypothesized that participants would adapt their movements to variations in charge strength, enabling accurate control over the stopping position of the repelled object.

4.6.2 Task Design and Conditions. Participants interacted with two virtual balls of the same charge polarity: a red held ball (b_h) and a green free ball (b_f). As participants moved b_h toward b_f, a simulated Coulomb repulsion pushed b_f away. The goal was to stop b_f as close as possible to a white target line, placed at 30, 35, or 40 cm along the virtual surface.

We varied the interaction strength $C_{hf} = k_e q_h q_f$ across three levels: 0.13, 0.18, and 0.23. These levels governed the magnitude of the repulsive force:

$$F_{\text{repulsive}} = \frac{C_{hf}}{r^2}$$

where r is the distance between b_h and b_f. Higher values of C_{hf} produced stronger forces at greater distances, reducing the physical movement needed to displace b_f.

4.6.3 Interaction Procedure. Each trial began with TrueForce aligning the physical proxy with the starting location of b_h. The spring was precompressed to match the repulsive force at rest, based on the initial r. The system then unlocked the pawl, and participants were instructed to approach and push b_h toward b_f using any comfortable hand motion.

As b_h approached b_f, participants felt increasing resistance. Once the repulsive force exceeded the static friction threshold, b_f moved toward the target. Participants were asked to observe the outcome and adjust their motion across repetitions.

Each C_{hf} condition included 15 trials (5 per line distance), and the order was partially randomized. The first block always used $C_{hf} = 0.18$ for calibration; the remaining blocks used $C_{hf} = 0.13$ and 0.23 in random order. An example trial flow is shown in Fig. 10a.

4.6.4 Modeling and Feedback Rendering. The force applied to the user was computed based on the repulsive field between b_h and b_f. The free ball's position and velocity were updated using a fourth-order Runge-Kutta (RK4) integrator to ensure smooth trajectories. Friction on b_f was

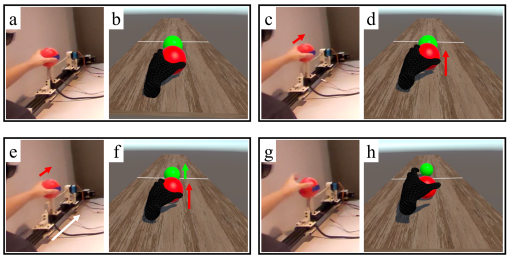

(a) Trial flow in Experiment 2: (a–b) initial alignment; (c–d) increasing repulsion; (e–f) b_f begins to move; (g–h) user observation for calibration.

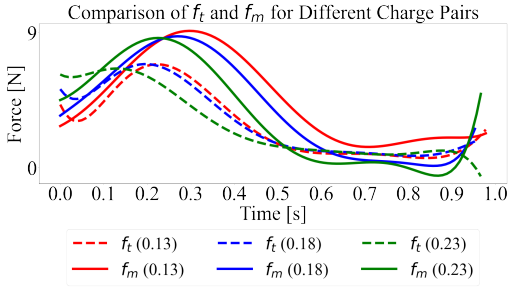

(b) Comparison of repulsive target force f_t and measured force f_m. The system accurately follows force rise but lags during decay.

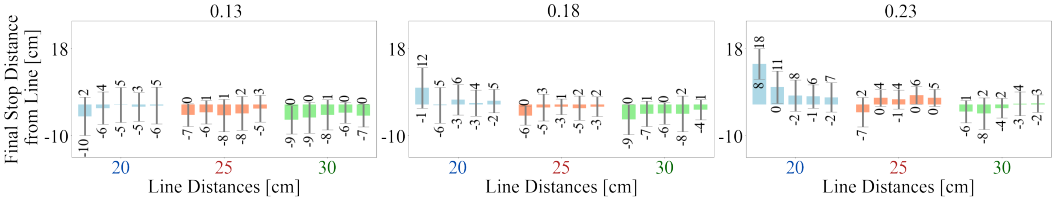

(c) Final distance between b_f and target across trials. Each marker represents the mean error across all 29 participants for a given line distance within that trial group, with whiskers indicating ±1 standard deviation. Error decreased after 2–3 trials in most blocks.

Fig. 10. Experiment 2 Summary: Electrostatic repulsion interaction. (a) shows the sequential steps of a trial, while (b) and (c) detail the force-tracking fidelity and adaptation performance across three charge levels.

modeled but friction on b_h was ignored to isolate the repulsion experience. The target force, f_t, was defined as $F_{\text{repulsive}}$.

This target force was compared to the measured force f_m from the load cell, and the spring compression was adjusted in real time. Ball positions were synchronized with the headset via UDP at 1 ms latency, as in Experiment 1.

4.6.5 *Results and Data Analysis.*

System Specifications and Task Utility. Because the relationship between hardware specifications and physical concepts is critical for VR education, our results clarify the practical boundaries of TrueForce. The system is highly effective for phenomena that involve gradual force gradients (such as the electrostatic repulsion in Experiment 2) or lower-mass dynamics (100–350 g objects), where the 0.25 m/s speed and 14 N threshold are not fully saturated. However, as the 600 g condition revealed, high-mass or high-acceleration tasks that demand rapid force spikes up to 14 N exceed the device's dynamic capabilities, resulting in force dampening. Therefore, the current hardware is most useful as an educational tool for exploring deliberate, moderate-force interactions rather than high-speed or high-impact collisions.

Force Feedback Fidelity. Fig. 10b compares the computed repulsive force f_t with the measured force f_m for each charge level. The ETHD successfully tracked the rising phase of the force across all conditions. However, as in Experiment 1, f_m lagged behind f_t during the falling phase due to the ETHD's limited speed when retracting the spring.

Despite this limitation, the profiles remained consistent in shape and timing across conditions, suggesting that users employed similar strategies once familiar with the force model. The tracking accuracy and predictable decay highlight TrueForce's capability to simulate continuous, dynamic non-contact interactions.

Adaptation and Calibration. Fig. 10c shows stopping distances across trials. In early trials, participants frequently overshot the line for higher C_{hf} values due to the increased repulsion strength. Within a few repetitions, however, stopping error decreased and variance narrowed—especially in the $C_{hf} = 0.18$ condition, which served as calibration.

4.7 Experiment 3: Bouncing a Moving Object

4.7.1 Purpose and Hypothesis. This experiment evaluated TrueForce's ability to render inertial feedback when participants interacted with a dynamic object. Unlike Experiment 1, where the object was stationary, participants here bounced back a virtual ball moving toward them at a constant speed. We hypothesized that participants would still be able to adapt their input to guide the ball toward the target, despite the added complexity of interacting with a moving object.

4.7.2 Task Design and Conditions. Participants were asked to bounce the virtual ball so that it stopped as close as possible to a white line placed at 70, 80, or 90 cm from the starting point. The ball began 40 cm away from the participant and moved toward them at a constant speed of 20 cm/s. Participants could hit the ball at any point along its path. Training used a 250 g mass, and test trials used 100 g, 350 g, and 600 g masses. The static and rolling friction coefficients were 0.8 and 0.15, respectively.

To trigger the ball's motion, participants placed their hand inside a green cube at the original start position. This triggered the physical device and virtual ball to begin moving toward the participant at a fixed speed. Friction was disabled before contact to reduce complexity and focus participant attention on the bouncing interaction.

4.7.3 Interaction Procedure. Once the virtual ball began moving, the system waited for contact. When the applied force exceeded 0.5 N (to filter out noise), TrueForce synchronized the physical and virtual dynamics. Participants were instructed to avoid snapping gestures and instead use smooth, continuous contact, similar to Experiment 1. Fig. 11a shows a sample trial sequence, including both real and virtual views. No subjective mass identification questions were asked, as mass perception was evaluated in Experiment 1.

4.7.4 Modeling and Feedback Rendering. The physical interaction model from Experiment 1 was reused with a directional adjustment. Since the ball approached the user, the net acceleration was $\frac{f_m+\mu_r mg}{m}$

The implementation also adjusted how velocity was updated during direction changes. If the object stopped and reversed direction within a time step, only the remaining time was used to compute the new velocity:

$$v^{\text{new}} = \frac{f_m - \mu_r mg}{m} \cdot \left(\Delta t - \frac{v^{\text{prev}}}{a^{\text{prev}}}\right)$$

4.7.5 Results and Data Analysis.

Force Feedback Fidelity. Fig. 11b shows the fitted target force f_t and measured force f_m curves. Compared to Fig. 9b, f_t values were notably smaller, reflecting that the ball's initial motion required less force to reverse. Rolling friction aided deceleration, which helped reduce the discrepancy between f_t and f_m.

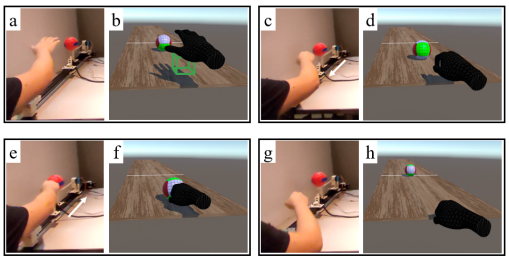

(a) Trial sequence in Experiment 3: (a,b) user prepares; (c,d) ball approaches; (e,f) contact; (g,h) result after rebound.

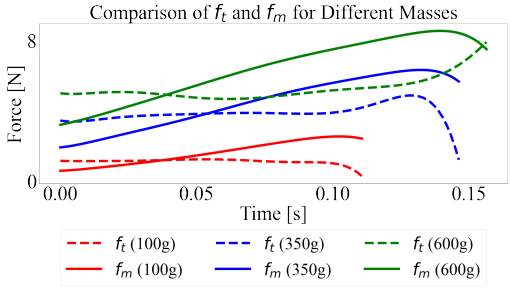

(b) Comparison of target and measured force over time across ball masses.

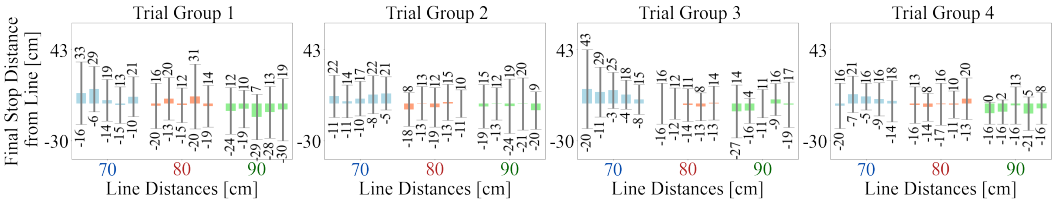

(c) Final distance from the target line. Each marker represents the mean error across all 29 participants for a given line distance within that trial group, with whiskers indicating ±1 standard deviation. The first 15 trials (Trial Group 1) represent the 250 g training phase. Each cluster represents a different mass and target distance.

Fig. 11. Experiment 3 Summary: Dynamic interception of a moving ball. (a) illustrates the interaction phases, while (b) and (c) detail the force-tracking fidelity and adaptation performance.

Another difference was the interaction duration. While Experiment 1 saw roughly 0.2 s of contact time, bouncing interactions here lasted around 0.15 s due to the higher relative speed and rebound dynamics. This resulted in a sharper decline in both f_t and f_m, especially for heavier balls. Overall, while the task introduced more timing uncertainty, it required less force and produced tighter alignment between target and measured responses.

Adaptation Performance. Fig. 11c shows the final distance from the white line across trials. Compared to Experiment 1, participants exhibited a wider spread of responses, especially during the early trials of each mass condition. This suggests a steeper learning curve due to the added challenge of timing the interaction with a moving object.

Participants often commented on the difficulty of deciding when to hit the ball. Some struck early; others hesitated, leading to more variability and slower convergence on an optimal strategy.

5 Discussion

Pedagogical Applicability and Dimensionality. The hardware constraints of the TrueForce prototype—specifically the single-axis compression of the spring—shape its educational utility. By restricting feedback to a single vector, the system acts as a "physical workbench" for 1D Newtonian mechanics. It is highly effective for teaching concepts where force and motion are co-linear, such as linear momentum ($p = mv$), static vs. kinetic friction, and 1D Coulombic repulsion. However, this dimensionality is a inherent limitation: the 1D mapping prevents the exploration of more complex 3D phenomena like torque, angular momentum, or off-axis collisions. There is a fundamental

trade-off: the current hardware simplifies the sensorimotor mapping to help students internalize specific laws without confounding spatial variables, but it underutilizes VR's inherent 3D expressive potential.

Adaptation and Calibration. Our three experiments demonstrate that TrueForce can render diverse force–time profiles while allowing participants to adapt rapidly to new interaction dynamics. In Experiments 1 and 2, participants reduced their errors within the first 2–3 trials, reaching stable performance without explicit feedback. This fast calibration aligns with prior evidence that humans can internalize new force–motion mappings within just a few exposures [Jones 2003]. By the third trial in Experiment 1, most users already brought the virtual ball within 20 cm of the target line, and in Experiment 2, overshoot errors diminished quickly even under stronger repulsion levels. Such rapid adaptation suggests that TrueForce can help learners intuitively grasp the relationships between force, mass, and motion, which is central to physics education. This pattern of rapid calibration is particularly valuable for learning and training contexts: while our current evaluation focuses on task performance and adaptation speed, these metrics are vital precursors to conceptual learning. The observed rapid calibration suggests that users can effectively internalize the system's force-motion mappings. While further longitudinal studies with pre- and post-tests are required to confirm conceptual mastery, the high fidelity and low error rates achieved here provide a robust sensorimotor foundation upon which such physical understanding can be built.

Force Fidelity and Perception. Force fidelity also proved sufficient for perceptual realism in most conditions. While our system utilizes a 0.5 N control threshold [Jones 2003] to trigger motor adjustments, the actual dynamic tracking error frequently exceeded this value across all experiments, particularly during the initial force onset and rapid decay phases. However, despite these dynamic discrepancies, participants still adapted rapidly and achieved the task goals. This indicates that effective perceptual tolerance in visually guided, dynamic interactions is more forgiving than in isolated static force discrimination tasks. However, participants still adapted and achieved the task goals, indicating that effective perceptual tolerance in visually guided, dynamic interactions is more forgiving than in isolated force discrimination tasks. This aligns with prior evidence that vision can dominate over haptics when cues conflict, effectively raising the functional threshold for force mismatch detectability [Slater 2009].

Limitations and Future Real-World Application. Beyond the dimensional constraints discussed above, a few limitations should be noted. Learning effects likely reduced independence across conditions, and the 1D prototype may have influenced realism compared to vertical baselines. These constraints limit generalizability but also clarify directions for future work, such as counterbalanced designs and 3D motion.

Taken together, these results suggest that TrueForce can support real-world applications where rapid, intuitive adaptation to physical laws is valuable. In its current form, the system is well suited for educational settings, such as teaching momentum transfer, Coulomb's law, or conservation principles through hands-on interaction without physical lab equipment. With extensions to multi-DOF actuation, TrueForce could enable more complex 3D tasks, including deflections in arbitrary directions, momentum exchange between colliding bodies, or even the study of soft-object interactions. Such applications directly address the paper's original motivation: providing learners with tangible, physically meaningful interactions that bridge abstract formulas and embodied experience.

6 Conclusion, Limitation, and Future Work

This work demonstrates how TrueForce extends grounded haptic devices with compliant, perceptually aligned force rendering across static, repulsive, and dynamic tasks.

Hardware Trade-offs in Force Rendering. Our experiments highlight physical limitations in the current ETHD design. Because force rendering is coupled to spring compression, there exists a trade-off between maximum renderable force, smoothness of transitions, and system responsiveness. Softer springs improve comfort and reduce vibration, but limit the system's ability to update forces quickly. Conversely, stiffer springs support larger force ranges but can degrade the user experience through abrupt force changes. Our findings show that TrueForce performs reliably up to 25 cm/s hand speeds, but struggles with faster interactions—a limitation for more aggressive or time-critical scenarios.

Opportunities for Mechanism Improvement. A promising direction is to decouple force modulation from spring compression. Instead of relying solely on mechanical compliance, integrating rapid, low-latency actuators could provide better control. For example, electrostatic clutches [Hinchet and Shea 2022] and magnetorheological (MR) brakes [Gang et al. 2019] offer fast, energy-efficient force adjustment with minimal mechanical complexity. These could reduce latency while maintaining soft, smooth contact. Such upgrades would also make the second assembly (for repositioning) modular, allowing future integration with other ETHDs such as robotic arms or Cartesian robots.

Toward Multi-DOF Interaction. To fully realize VR's 3D educational potential, future work must bridge our 1D force rendering with unconstrained spatial freedom. Generalized 3D interactions require six additional degrees of freedom for multi-axis force and spatial manipulation, building on our 1D linear compliance strategies. Systems like Force Dimension Omega (https://www.forcedimension.com/products/omega) could provide multi-axis force input, while a robotic arm manages 3D translation. Integrating these components would dynamically realign the compression axis to any 3D contact vector, enabling the study of complex phenomena like oblique impacts or rotational dynamics, thereby overcoming our current hardware constraints.

Educational Evaluation. A limitation of this study is the reliance on kinematic and force data rather than subjective assessments or standardized physics learning tests. While we have demonstrated that TrueForce supports high-fidelity physical interaction, future work will evaluate its pedagogical efficacy through longitudinal classroom studies to measure conceptual knowledge transfer.

Acknowledgments

This material is based upon work supported by the United States National Science Foundation under Awards No. 2212200, 2318657, 2309564, 2506783, and 2417510.

References

Elodie Bouzbib and Gilles Bailly. 2022. " Let's Meet and Work it Out": Understanding and Mitigating Encountered-Type of Haptic Devices Failure Modes in VR. In *2022 IEEE Conference on Virtual Reality and 3D User Interfaces (VR)*. IEEE, 360–369.

Yang Chen, Hamed Alimohammadzadeh, Shahram Ghandeharizadeh, and Heather Culbertson. 2024. Force-Feedback Through Touch-based Interactions With A Nanocopter. In *2024 IEEE Haptics Symposium (HAPTICS)*. IEEE, 271–277.

Shaozhang Dai, Jim Smiley, Tim Dwyer, Barrett Ens, and Lonni Besancon. 2022. RoboHapalytics: a robot assisted haptic controller for immersive analytics. *IEEE Transactions on Visualization and Computer Graphics* 29, 1 (2022), 451–461.

Laura Freina and Michela Ott. 2015. A literature review on immersive virtual reality in education: state of the art and perspectives. In *The international scientific conference elearning and software for education*, Vol. 1. 10–1007.

Han Gyeol Gang, Seung-Bok Choi, and Jung Woo Sohn. 2019. Experimental performance evaluation of a MR brake-based haptic system for teleoperation. *Frontiers in Materials* 6 (2019), 25.

Nur Al-huda Hamdan, Adrian Wagner, Simon Voelker, Jürgen Steimle, and Jan Borchers. 2019. Springlets: Expressive, flexible and silent on-skin tactile interfaces. In *Proceedings of the 2019 CHI Conference on Human Factors in Computing Systems*. 1–14.

Viviane Herdel, Lee J Yamin, and Jessica R Cauchard. 2022. Above and beyond: A scoping review of domains and applications for human-drone interaction. In *Proceedings of the 2022 CHI Conference on Human Factors in Computing Systems*. 1–22.

Ronan J Hinchet and Herbert Shea. 2022. Glove-and sleeve-format variable-friction electrostatic clutches for kinesthetic haptics. *Advanced Intelligent Systems* 4, 12 (2022), 2200174.

Felix Huppert, Gerold Hoelzl, and Matthias Kranz. 2021. GuideCopter-A precise drone-based haptic guidance interface for blind or visually impaired people. In *Proceedings of the 2021 CHI Conference on Human Factors in Computing Systems*. 1–14.

Lynette A Jones. 2003. Perceptual constancy and the perceived magnitude of muscle forces. *Experimental Brain Research* 151 (2003), 197–203.

Alexander Kalus, Johannes Klein, Tien-Julian Ho, Lee-Ann Seegets, and Niels Henze. 2024. MobileGravity: Mobile Simulation of a High Range of Weight in Virtual Reality. In *Proceedings of the CHI Conference on Human Factors in Computing Systems*. 1–13.

Yaesol Kim, Siyeon Kim, Uran Oh, and Young J Kim. 2020. Synthesizing the roughness of textured surfaces for an encountered-type haptic display using spatiotemporal encoding. *IEEE Transactions on Haptics* 14, 1 (2020), 32–43.

Yilong Lin, Peng Zhang, Eyal Ofek, and Seungwoo Je. 2024. ArmDeformation: Inducing the Sensation of Arm Deformation in Virtual Reality Using Skin-Stretching. In *Proceedings of the CHI Conference on Human Factors in Computing Systems*. 1–18.

Pedro Lopes, Alexandra Ion, and Patrick Baudisch. 2015. Impacto: Simulating physical impact by combining tactile stimulation with electrical muscle stimulation. In *Proceedings of the 28th annual ACM symposium on user interface software & technology*. 11–19.

Thomas H Massie, J Kenneth Salisbury, et al. 1994. The phantom haptic interface: A device for probing virtual objects. In *Proceedings of the ASME winter annual meeting, symposium on haptic interfaces for virtual environment and teleoperator systems*, Vol. 55. Chicago, IL, 295–300.

Alex Mazursky, Jas Brooks, Beza Desta, and Pedro Lopes. 2024. ThermalGrasp: Enabling Thermal Feedback even while Grasping and Walking. In *2024 IEEE Conference Virtual Reality and 3D User Interfaces (VR)*. IEEE, 342–353.

Victor Mercado, Maud Marchai, and Anatole Lécuyer. 2020. Design and evaluation of interaction techniques dedicated to integrate encountered-type haptic displays in virtual environments. In *2020 IEEE Conference on Virtual Reality and 3D User Interfaces (VR)*. IEEE, 230–238.

Victor Mercado, Maud Marchal, and Anatole Lécuyer. 2019. Entropia: towards infinite surface haptic displays in virtual reality using encountered-type rotating props. *IEEE transactions on visualization and computer graphics* 27, 3 (2019), 2237–2243.

Victor Rodrigo Mercado, Ferran Argelaguet, Géry Casiez, and Anatole Lécuyer. 2022. Watch out for the Robot! Designing Visual Feedback Safety Techniques When Interacting With Encountered-Type Haptic Displays. *Frontiers in Virtual Reality* 3 (2022), 928517.

Víctor Rodrigo Mercado, Maud Marchal, and Anatole Lécuyer. 2021. "haptics on-demand": A survey on encountered-type haptic displays. *IEEE Transactions on Haptics* 14, 3 (2021), 449–464.

Soroosh Mortezapoor, Khrystyna Vasylevska, Emanuel Vonach, and Hannes Kaufmann. 2023. CoboDeck: A Large-Scale Haptic VR System Using a Collaborative Mobile Robot. In *2023 IEEE Conference Virtual Reality and 3D User Interfaces (VR)*. IEEE, 297–307.

Voicu Popescu, Alejandra Magana, and Bedrich Benes. 2023. Towards Immersive Visualization for Large Lectures: Opportunities, Challenges, and Possible Solutions. In *The 44th Annual Conference of the European Association for Computer Graphics, Education Track, EG2023*.

Javier Posselt, Lionel Dominjon, A Bouchet, and A Kemeny. 2017. Toward virtual touch: Investigating encounter-type haptics for perceived quality assessment in the automotive industry. In *Proceedings of the 14th Annual EuroVR Conference, Laval, France*. 12–14.

Nico Rutten, Wouter R Van Joolingen, and Jan T Van Der Veen. 2012. The learning effects of computer simulations in science education. *Computers & education* 58, 1 (2012), 136–153.

Vivian Shen, Tucker Rae-Grant, Joe Mullenbach, Chris Harrison, and Craig Shultz. 2023. Fluid reality: High-resolution, untethered haptic gloves using electroosmotic pump arrays. In *Proceedings of the 36th Annual ACM Symposium on User Interface Software and Technology*. 1–20.

Alejandro Jarillo Silva, Omar A Domínguez Ramirez, Vicente Parra Vega, and Jesus P Ordaz Oliver. 2009. Phantom omni haptic device: Kinematic and manipulability. In *2009 Electronics, Robotics and Automotive Mechanics Conference (CERMA)*. IEEE, 193–198.

Mel Slater. 2009. Place illusion and plausibility can lead to realistic behaviour in immersive virtual environments. *Philosophical Transactions of the Royal Society B: Biological Sciences* 364, 1535 (2009), 3549–3557.

Ryo Suzuki, Hooman Hedayati, Clement Zheng, James L Bohn, Daniel Szafir, Ellen Yi-Luen Do, Mark D Gross, and Daniel Leithinger. 2020. Roomshift: Room-scale dynamic haptics for vr with furniture-moving swarm robots. In *Proceedings of the 2020 CHI conference on human factors in computing systems*. 1–11.

Yudai Tanaka, Alan Shen, Andy Kong, and Pedro Lopes. 2023. Full-hand electro-tactile feedback without obstructing palmar side of hand. In *Proceedings of the 2023 CHI Conference on Human Factors in Computing Systems*. 1–15.

Andre Zenner and Antonio Krüger. 2017. Shifty: A weight-shifting dynamic passive haptic proxy to enhance object perception in virtual reality. *IEEE transactions on visualization and computer graphics* 23, 4 (2017), 1285–1294.

Yuqi Zhou and Voicu Popescu. 2023. Dynamic redirection for vr haptics with a handheld stick. *IEEE Transactions on Visualization and Computer Graphics* 29, 5 (2023), 2753–2762.

Yuqi Zhou and Voicu Popescu. 2025. Dynamic redirection for safe interaction with ethd-simulated virtual objects. *IEEE Transactions on Visualization and Computer Graphics* (2025).